ES Materials & Manufacturing

Journal:	ES Materials & Manufacturing
Manuscript ID:	ES-MM-2019-0017.R1
Article Type:	Communication
Date of Submission:	5/4/2019
Date of acceptance:	12/8/2019

Accepted Manuscript

Title: "Sintering Behavior and Microwave Dielectric Properties of Low-Loss $Li_6Mg_7Zr_3O_{16}$ Ceramics Doped with Different LiF Additives"

Author(s): H.R. Tian, C.F. Xing, H.T. Wu, Z.H. Wang

To be cited as: *ES Mater. Manuf.*, 2019, in press, DOI: 10.30919/esmm5f603

* Corresponding author.
Tel.: +86 531 82769782; fax: +86 531 87974453.
E-mail address: mse_wuht@ujn.edu.cn (H.T. Wu).

Sintering Behavior and Microwave Dielectric Properties of Low-Loss $Li_6Mg_7Zr_3O_{16}$ Ceramics Doped with Different LiF Additives

H.R. Tian[a], C.F. Xing[a], H.T. Wu[a,*], Z.H. Wang[b,*]

[a]School of Materials Science and Engineering, University of Jinan, Jinan 250022, China

[b]School of Materials Science and Engineering, Qilu University of Technology (Shandong Academy of Sciences), Jinan, 250353, PR China

Abstract

The $Li_6Mg_7Zr_3O_{16}$ samples were prepared with the pure cubic phase at sintering temperatures of 1300-1550°C using the traditional solid state method in our previous work. Sintering characteristics and microwave properties were investigated as a function of sintering temperatures. The samples sintered at 1500 °C showed the best properties of the $Q{\cdot}f$ value of 81,284 GHz (at 8.94 GHz), dielectric constant value of 14.22 and the τ_f value of -21.56 ppm/°C. Now complex permittivity value of $Li_6Mg_7Zr_3O_{16}$ ceramic sintered at 1500 °C were characterized by the infrared spectra based on the classical harmonic oscillator model. In order to reduce the sintering temperature, lithium fluoride were used as sintering additives, and then the apparent densities, phase compositions and dielectric properties of $Li_6Mg_7Zr_3O_{16}$ -x (0 wt% LiF $\leq x \leq$ 5 wt% LiF) were discussed as a function of lithium fluoride additions. As a result the densification temperatures for $Li_6Mg_7Zr_3O_{16}$-5 wt% LiF were reduced to be 1100 °C, which were significantly lower than that of the matrix (1500 °C). Excellent microwave dielectric properties were obtained in $Li_6Mg_7Zr_3O_{16}$-5 wt% LiF ceramics sintered at 1100 °C with ε_r=13.67, $Q{\cdot}f$=132,600 GHz (at 9.26 GHz) and τ_f=-18.89 ppm/°C.

Keywords: Low-temperature sintering; $Li_6Mg_7Zr_3O_{16}$ ceramics; Infrared spectra; Microwave dielectric properties; LiF addition

1. Introduction

With the rapid development of the wireless communication industry, microwave dielectric ceramics with high performances have been widely investigated and used for microwave components, such as filters, antennas, oscillators and resonators.[1-4] To satisfy the specific requirements of current and future microwave devices, high-performance ceramics with an appropriate dielectric constant (ε_r), a high quality factor ($Q{\cdot}f$) and a near-zero temperature coefficient of the resonant frequency (τ_f) are required. Nowadays a great number of new materials with excellent microwave dielectric properties have been widely investigated, such as the $ReNbO_4$ system,[5-7] Mo-based

microwave dielectric ceramics,[8-10] and the rock salt systems or others[11-13]. For example, the $LaNbO_4$-0.5MgO ceramics sintered at 1425 °C possessed excellent performance: ε_r=19.8, $Q{\cdot}f$=94,440 GHz, τ_f=6.1 ppm/°C.[6] The $La_2(Zr_{1-x}Ti_x)_3(MoO_4)_9$ ceramics achieved the best dielectric properties with ε_r= 10.33, $Q{\cdot}f$= 80,658 GHz and τ_f= -16.80 ppm/℃.[10]

It was found in our previous work that the Li_2ZrO_3-MgO system sintered at 1500 °C exhibited excellent dielectric properties of ε_r=12.65, $Q{\cdot}f$=165,924 GHz and τ_f=-34.66 ppm/°C.[11] However, the high sintering temperature restricted its possible applications. In order to lower the sintering temperature, it is one of efficient methods to add or substitute sintering aids, such as LiF, CuO, H_3BO_3, Bi_2O_3 and glass in the past report.[14-24] For example, when LiF content increased from 0 to 5 wt%, the optimum sintering temperature of $CaMgSi_2O_6$ ceramics reduced from 1250 °C to 900 °C.[18] Zhou et al. reported that $Bi_2(Li_{0.5}Ta_{1.5})O_7$ ceramics were densified at 1025 °C, the sintering temperature was lowered to 920 °C by the addition of 2 mol% excess Bi_2O_3.[21] The H_3BO_3-doping in $(1-x)LiAl_{0.98}(Zn_{0.5}Si_{0.5})_{0.02}O_2$ + $xCaTiO_3$ ($0.05 \le x \le 0.20$) ceramics was used to decrease the sintering temperature from 1150 °C to 900 °C.[23] Among them, LiF is one of inexpensive as well as the most effective sintering additives to reduce the sintering temperature of microwave dielectric materials. Hence, a conventional solid-state reaction method was used to prepare $Li_6Mg_7Zr_3O_{16}$ ceramics doped with different amounts of LiF. The microstructures, sintering characteristics as well as microwave dielectric properties of $Li_6Mg_7Zr_3O_{16}$-x (0 wt% LiF $\le x \le$ 5 wt% LiF) were investigated scientifically.

2. Experimental procedure

$Li_6Mg_7Zr_3O_{16}$ compositions was prepared using reagent-grade powders of MgO (99.99%, Aladdin), Li_2CO_3 (99.99%, Aladdin) and ZrO_2 (99.99%, Aladdin). The raw materials were mixed by ball-milling for 24 h with zirconia balls and alcohol. The resulting slurry was dried after milling. After drying, powders were calcined at 1100 °C for 2 h thereafter. After calcination, powders were mixed together with 0-5 wt% LiF additives and then re-milled for 24 h. Powders were ground with 8 wt% PVA, and pressed into cylinders in a steel die thereafter. Finally, the matrix was sintered at 1300-1550 °C for 4 h in air, and $Li_6Mg_7Zr_3O_{16}$-x (1 wt% LiF $\le x \le$ 5 wt% LiF) ceramics were sintered at 800-1150 °C.

The X-ray diffractometer (Brucker D8) was used to analyse crystal structures of $Li_6Mg_7Zr_3O_{16}$-x (0 wt% LiF $\le x \le$ 5 wt% LiF). IR reflectivity spectrum was obtained via a FTIR spectrometer (Bruker IFS 66v). Microstructures of sintered samples were observed by the SEM (FeSEM Quanta 250, FEI Co., USA). The ε_r values was measured using

Hakki-Coleman dielectric resonator method in TE_{011} resonant mode by A network analyzer (N5234A, Agilent Co., USA),[25] the unloaded quality factor was measured using TE_{01d} mode by the cavity method.[26] τ_f values were calculated at 25-85 °C using the following equation:

$$\tau_f = \frac{f_1 - f_0}{f_0 \times \Delta T} \times 10^6 \, (ppm/°C) \quad (1)$$

where f_0 and f_1 represented the resonant frequency at 25 °C as well as 85 °C, respectively.

3. Results and discussion

The X-ray diffraction patterns of $Li_6Mg_7Zr_3O_{16}$ samples were shown in Fig.1.[11] From the recorded XRD patterns, $Li_6Mg_7Zr_3O_{16}$ with a cubic structure (JCPDS care no. 45-0946) was identified. Moreover, no other phases could be detected, indicating that the pure cubic $Li_6Mg_7Zr_3O_{16}$ was formed in the temperature range 1300-1500 °C. The illustrations of $Li_6Mg_7Zr_3O_{16}$ crystal were exhibited in Fig. 2. It was noted that the oxygen octahedral sites were occupied by the Li, Mg and Zr atoms. In the structure, the cations (Li, Mg and Zr) occupied the 4a Wyckoff position, and O anions occupied the 4b Wyckoff position. According to complex chemical bond theory, the result of the decomposition of $Li_6Mg_7Zr_3O_{16}$ was exhibited in Eq. (2).[27-29] Fig. 2 displayed the charge distribution of ions and the coordination number in $Li_6Mg_7Zr_3O_{16}$ samples. The coordination numbers of Li, Mg, and Ti were 6. The effective valences of cations were Z_{Li}=1, Z_{Mg}=2 and Z_{Ti}=4, while effective valence of the anion (O) was closely related to the charge balance in the specific chemical bond, where Z_O=-1 in Li-O bond, Z_O=-2 in Mg-O bond as well as Z_O=-4 in Ti-O bond.

$$\begin{aligned} Li_6Mg_7Zr_3O_{16} &\rightarrow (Li/Mg/Zr)_{16}O_{16} \\ &\rightarrow Li_6O_6 + Mg_7O_7 + Zr_3O_3 \end{aligned} \quad (2)$$

Based on our previous work[11], the shrinkage ratios and the apparent densities of the $Li_6Mg_7Zr_3O_{16}$ samples could reach the saturated values at 1500 °C during the temperature increasing from 1300 to 1550°C. Correspondingly according to the curves of dielectric constants and quality factors for $Li_6Mg_7Zr_3O_{16}$ samples from 1300 to 1550 °C, it was noted that dielectric constant increased from 13.37 to 14.28 with increasing temperature, which was caused by the elimination of pores. Then, the dielectric constant reached a saturated value in the temperature range 1500-1550 °C. The best $Q \cdot f$ value of $Li_6Mg_7Zr_3O_{16}$ samples increased to 81,284 GHz (at 8.94 GHz) as the sintering temperature increased to 1500 °C. Moreover, the τ_f value of $Li_6Mg_7Zr_3O_{16}$ sample sintered at the optimum sintering temperature (1500 °C) was -21.56 ppm/°C.

Fig.3 presented the IR reflectivity spectrum of $Li_6Mg_7Zr_3O_{16}$ sintered at 1500 °C. Eq. (3) is used to calculate $\varepsilon^*(\omega)$ (the complex dielectric permittivity) based on the model of classical harmonic oscillator, and R (the complex reflectivity) can be obtained as Eq. (4)[30,31]

$$\varepsilon^*(\omega) = \varepsilon_\infty + \sum_{j=1}^{n} \frac{\omega_{pj}^2}{\omega_{oj}^2 - \omega^2 + i\omega\gamma_j} \tag{3}$$

$$R = \left| \frac{1 - \sqrt{\varepsilon^*(\omega)}}{1 + \sqrt{\varepsilon^*(\omega)}} \right|^2 \tag{4}$$

where ω_{oj}, ω_{pj} and ε_∞ are the transverse frequency, intensity and dielectric constant, respectively; n as well as γ_j are the number of transverse phonon modes and damping factor, respectively. In addition, the following formulas were used to calculate the *tan δ* (dielectric loss tangent):

$$\tan\delta = \frac{\varepsilon''}{\varepsilon'} = \frac{\sum_{j=1}^{n} \Delta\varepsilon_j (\gamma_j \omega) / \omega_{oj}^2}{\varepsilon_\infty + \sum_{j=1}^{n} \Delta\varepsilon_j} \tag{5}$$

$$\varepsilon' = \varepsilon_\infty + \sum_{j=1}^{n} \frac{\omega_{pj}^2}{\omega_{oj}^2} = \varepsilon_\infty + \sum_{j=1}^{n} \Delta\varepsilon_j \tag{6}$$

Fig.4 showed the complex permittivity values and fitted IR reflectivity spectra. As shown in Table 1, there were five internal modes. The extra-polated dielectric loss and permittivity of $Li_6Mg_7Zr_3O_{16}$ were 0.44×10^{-4} and 22.88, respectively. These calculated results were comparable with the measured ones. Hence, the microwave dielectric properties of $Li_6Mg_7Zr_3O_{16}$ were mainly related to the absorptions of phonon oscillation.

The apparent densities of $Li_6Mg_7Zr_3O_{16}$-x (1 wt% LiF ≤ x ≤ 5 wt% LiF) ceramics were plotted in Fig. 5. Apparent densities of $Li_6Mg_7Zr_3O_{16}$-x (1 wt% LiF ≤ x ≤ 5 wt% LiF) ceramics initially increased to the maximum values at their optimum temperatures and then reached saturation with further increasing the temperatures. The apparent densities of $Li_6Mg_7Zr_3O_{16}$-x (3 wt% LiF ≤ x ≤ 5 wt% LiF) ceramics were higher than that of $Li_6Mg_7Zr_3O_{16}$-x (1 wt% LiF ≤ x ≤ 2 wt% LiF). Especially, the apparent densities of $Li_6Mg_7Zr_3O_{16}$-x wt% LiF (x=5) increased to 3.54 g/cm^3 approximately at 900 °C, which was similar to that (3.66 g/cm^3) of $Li_6Mg_7Zr_3O_{16}$ sintered at 1500 °C. In addition, the apparent density increased with increasing x value. Therefore, LiF additive was an effective sintering aid to lower sintering temperature of $Li_6Mg_7Zr_3O_{16}$ system.

Fig. 6 showed XRD patterns of $Li_6Mg_7Zr_3O_{16}$-x (1 wt% LiF ≤ x ≤ 5 wt% LiF) samples sintered at 1100 °C. For $Li_6Mg_7Zr_3O_{16}$-x (1 wt% LiF ≤ x ≤ 2 wt% LiF) compositions, main cubic phase was observed. The second phases were ZrO_2 and Li_2MgZrO_4 for x=1 and x=2, respectively. As the LiF content increased from 3 to 5 wt%, a single phase was formed in the entire composition range, suggesting that $Li_6Mg_7Zr_3O_{16}$-x (x=3-5 wt% LiF) was a complete solid solution with a cubic structure. Typical SEM micrographs of $Li_6Mg_7Zr_3O_{16}$-x (1 wt% LiF ≤ x ≤ 5 wt% LiF) samples were demonstrated in Fig. 7(a-e). The porous structures were revealed in the surface of samples. It was observed that relatively dense microstructures were obtained for $Li_6Mg_7Zr_3O_{16}$ sample doped with 5 wt% LiF.

Fig. 8 illustrated the variation in the dielectric constants for $Li_6Mg_7Zr_3O_{16}$-x (1 wt% LiF ≤ x ≤ 5 wt% LiF). Generally, ε_r value is closely related to density and secondary phase. For the specimens with x =1- 2, dielectric constants had relatively lower values compared with that of $Li_6Mg_7Zr_3O_{16}$-x (3 wt% LiF ≤ x ≤ 5 wt% LiF) ceramics, which might be caused by the second phases and the apparent densities. For x=3-5, the XRD patterns in Fig. 6 showed a pure phase. Therefore, ε_r values of $Li_6Mg_7Zr_3O_{16}$-x (3 wt% LiF ≤ x ≤ 5 wt% LiF) were mainly dependent on densities. With temperature increasing from 900 to 1100 °C, it was seen that the ε_r values of $Li_6Mg_7Zr_3O_{16}$-x (3 wt% LiF ≤ x ≤ 5 wt% LiF) remained stable at a given LiF content, indicating that ε_r value was not significantly influenced by the temperature for the sample with high densification.[32]

Quality factors of $Li_6Mg_7Zr_3O_{16}$-x (1 wt% LiF ≤ x ≤ 5 wt% LiF) samples were exhibited in Fig. 9. Quality factors are mainly influenced by the intrinsic losses (lattice vibration mode) and extrinsic losses (densification of the samples, second phases as well as grain morphology).[33,34] Factors influencing the quality factors of $Li_6Mg_7Zr_3O_{16}$-x (1 wt% LiF ≤ x ≤ 5 wt% LiF) ceramics were the extrinsic ones mainly contributing to the densification. Quality factors of $Li_6Mg_7Zr_3O_{16}$-x (3 wt% LiF ≤ x ≤ 5 wt% LiF) ceramics were higher than that of $Li_6Mg_7Zr_3O_{16}$-x (1 wt% LiF ≤ x ≤ 2 wt% LiF) samples, which might be related to the densities and the second phases of the ceramics. For instance, quality factor of $Li_6Mg_7Zr_3O_{16}$-x wt% LiF (x=1) increased from 8,200 GHz (at 10.49 GHz) to 75,500 GHz (at 10.67 GHz) with increasing temperature, while the maximum quality factors of $Li_6Mg_7Zr_3O_{16}$-5 wt% LiF ceramics reached to 132,600 GHz (at 9.26 GHz) at 1100 °C, which was higher than that (81,277 GHz) of $Li_6Mg_7Zr_3O_{16}$. Therefore, it could be found that the appropriate LiF contents might improve the sintering characteristis without any deterioration on quality factors of $Li_6Mg_7Zr_3O_{16}$ ceramics.

Microwave dielectric properties of $Li_6Mg_7Zr_3O_{16}$-x (1 wt% LiF ≤ x ≤ 5 wt% LiF) sintered at 1100 °C were exhibited in Fig. 10. As LiF content increased from 1 to 5 wt%, the ε_r value and the quality factor showed an upward

tendency due to the increase of density. It is well known that the τ_f values are governed by the composition, the additives and the second phase of the materials.[35] The τ_f value initially decreased from -19.5 ppm/°C to -27.2 ppm/°C with increasing x value, and then increased to -18.89 ppm/°C, which might be affected by additives in this work. Typically, $Li_6Mg_7Zr_3O_{16}$-x wt% LiF (x=5) ceramic possessed a single phase with good properties of τ_f=-18.89 ppm/°C, $Q{\cdot}f$=132,600 GHz (at 9.26 GHz) and ε_r=13.67.

4. Conclusion

$Li_6Mg_7Zr_3O_{16}$-x (0 wt% LiF ≤ x ≤ 5 wt% LiF) samples were synthesized by the solid-state method. Appropriate amount of LiF additive improved the sinterability of the $Li_6Mg_7Zr_3O_{16}$ system. The sintering temperature of the ceramic was reduced with increasing LiF content, which was caused by the enhancement of the apparent density at low temperature by liquid phase sintering. The dielectric constants and quality factors increased gradually when temperatures and LiF additives increased. Compared with $Li_6Mg_7Zr_3O_{16}$ ceramics sintered at 1500°C, 5% LiF doped-$Li_6Mg_7Zr_3O_{16}$ samples could be sintered well at 1100°C with excellent properties of ε_r=13.67, $Q{\cdot}f$=132,600 GHz (at 9.26 GHz) as well as τ_f=-18.89 ppm/°C .

Acknowledgments

This work was supported by the National Natural Science Foundation of China (No. 51972143). The authors are thankful to the help of Professor Zhen Xing Yue and postdoctoral Jie Zhang on the measurement of microwave properties in Tsinghua University. The authors are also thankful to the administrators in IR beamline workstation of National Synchrotron Radiation Laboratory (NSRL) for the help in IR measurement.

References

[1] D. Zhou, W.B. Li, H.H. Xi, L.X. Pang and G.S. Pang, J. Mater. Chem. C., 2015, **3**, 2582-2588.

[2] Y. Wang, T.L. Tang, J.T. Zhang, W.S. Xia, L.W. Shi, J. Alloys Compd., 2019, **778**, 576-578.

[3] H.H. Guo, D. Zhou, W.F. Liu, L.X. Pang, D.W. Wang, J.Z. Su, Z.M. Qi, J. Am. Ceram. Soc., 2020, **103**, 423-431.

[4] W.S. Xia, F. Jin, M. Wang, X. Wang, G.Y. Zhang, L.W. Shi, J. Mater. Sci. Mater. Electron., 2016, **27**, 1100-1104.

[5] W.S. Xia, S.B. Zhang, T.L. Tang, Y. Wang, L.W. Shi, Physica B., 2019, **572**, 148-152.

[6] T.L. Tang, W.S. Xia, B. Zhang, Y. Wang, M.X. Li, L.W. Shi, J. Mater. Sci. Mater. Electron., 2019, **30**, 15293-15298.

[7] L.X. Pang, D. Zhou, J. Am. Ceram. Soc., 2019, **102**, 2278-2282.

[8] H.H Guo, D Zhou，L.X Pang, Z.M Qi, J. Eur. Ceram. Soc., 2019, **39**, 2365-2373.

[9] Y.H. Zhang, J.J. Sun, N. Dai, Z.C. Wu, H.T. Wu, C.H. Yang, J. Eur. Ceram. Soc., 2019, **39**, 1127-1131.

[10] Y.H. Zhang, H.T. Wu, J. Am. Ceram. Soc., 2019, **102**, 4092-4102.

[11] J.X. Bi, C.F. Xing, C.H. Yang and H.T. Wu, J. Eur. Ceram. Soc., 2018, **38**, 3840-3846.

[12] M.J. Wu, Y.C. Zhang, M.Q. Xiang, J. Adv. Ceram., 2019,**8**,228-237.

[13] A. Manan, Z. Ullah, A. S. Ahmad, A. Ullah, D.F. Khan, A. Hussain, M.U. Khan,2018,**7**,72-78.

[14] Z.W. Zhang, L. Fang, H.C. Xiang, M.Y. Xu, Y. Tang, H. Jantunen, C.C. Li, Ceram. Int., 2019, **45**, 10163-10169.

[15] Y. Wang, L.Y. Zhang, S.B. Zhang, W.S. Xia, L.W. Shi, Mater. Lett., 2018, **219**, 233-235.

[16] X.Q. Song, W. Lei, Y.Y. Zhou, T. Chen, S.W. Ta, Z.X. Fu, W.Z. Lu, J. Am. Ceram. Soc., https://doi.org/10.1111/jace.16795.

[17] X.Q. Song, K. Du, J. Li, X.K. Lan, W.Z. Lu, X.H. Wang, W. Lei, Ceram. Int., 2019, **45**, 279-286.

[18] Y.M. Lai, H. Su, G. Wang, X.L. Tang, X. Huang, X.F. Liang, H.W. Zhang, Y.X. Li, K. Huang, X.R. Wang, J. Am. Ceram. Soc., 2019, **102**, 1893-1903.

[19] W.S. Xia, L.Y. Zhang, Y. Wang, J.T. Zhang, R.R. Feng, L.W. Shi, J. Mater. Sci. Mater. Electron., 2017, **28**, 18437-18441.

[20] P. Zhang, M.M. Yang, H. Xie, M. Xiao, Z.T. Zheng, Mater. Chem. Phys., 2019, **227**, 130-133.

[21] D. Zhou, L.X. Pang, D.W. Wang, C. Li, B.B. Jin, I.M. Reaney, J. Mater. Chem. C., 2017, **5**, 10094-10098.

[22] J. Zhang, R.Z. Zuo, J. Song, Y.D. Xu, M. Shi, Ceram. Int., 2018, **44**, 2606-2610.

[23] X.K. Lan, J. Li, F. Wang, X.H. Wang, W.Z. Lu, M.Z. Hu, W. Lei, Int. J. Appl. Ceram., Tec. https://doi.org/10.1111/ijac.13368.

[24] H.I. Hsiang, C.C. Chen, S.Y. Yang, J. Adv. Ceram., 2019, **8**, 345-351.

[25] B.W. Hakki and P.D. Coleman, IRE Trans. Microw. Theory Tech., 1960, **8**, 402-410.

[26] W.E. Courtney, IEEE Trans. Microw. Theory Tech., 1970, **18**, 476-485.

[27] D.F. Xue and S.Y. Zhang, J. Phys.: Condens. Matter, 1996, **8**, 1949-1956.

[28] Z.J. Wu, Q.B. Meng and S.Y. Zhang, Phys. Rev. B, 1998, **58**, 958-962.

[29] Q.B. Meng, Z.J. Wu and S.Y. Zhang, J. Phys.: Condens. Matter, 1998, **1**, 85-88.

[30] J. Petzelt and S. Kamba, Mater. Chem. Phys., 2003, **79**, 175-180.

[31] K. Wakino, M. Murata and H. Tamura, J. Am. Ceram. Soc., 1986, **69**, 34-37.

[32] J. Li, Y. Han, T. Qiu and C. Jin, Mater. Res. Bull., 2012, **47**, 2375-2379.

[33] H.D. Xie, H.H. Xi, F. Li, C. Chen, X.C. Wang and D. Zhou, J. Eur. Ceram. Soc., 2014, **34**, 4089-4093.

[34] V.L. Gurevich and A.K. Tagantsev, Adv. Phys., 1991, **40**, 719-767.

[35] P. Zhang, Z.K. Song, Y. Wang, Y.M. Han, H.L. Dong and L.X. Li, J. Alloys Compd., 2013, **581**, 741-746.

Figures captions

Fig. 1 XRD patterns of $Li_6Mg_7Zr_3O_{16}$ ceramics sintered at 1300-1500 °C

Fig. 2 The schematic crystal structure of $Li_6Mg_7Zr_3O_{16}$ ceramic and the coordination number and charge distribution of ions in $Li_6Mg_7Zr_3O_{16}$ ceramic

Fig. 3 Measured (black line) and fitted (red line) IR reflectivity spectrum of $Li_6Mg_7Zr_3O_{16}$ ceramic sintered at 1500 °C

Fig. 4 Real and imaginary parts of complex permittivity for $Li_6Mg_7Zr_3O_{16}$ ceramic sintered at 1500 °C (points are measured values at microwave region)

Fig. 5 Apparent densities of the $Li_6Mg_7Zr_3O_{16}$-*x* wt% LiF (*x*=1-5) ceramics sintered at 800-1150 °C

Fig. 6 XRD patterns of $Li_6Mg_7Zr_3O_{16}$-*x* wt% LiF (*x*=1-5) ceramics sintered at 1100 °C in air

Fig.7 SEM micrographs of $Li_6Mg_7Zr_3O_{16}$-*x* wt% LiF (*x*=1-5) ceramics sintered at 1100 °C (a-e corresponding to *x*=1, 2, 3, 4, 5)

Fig. 8 Dielectric constants of $Li_6Mg_7Zr_3O_{16}$-*x* wt% LiF (*x*=1-5) ceramics sintered at 800-1150 °C

Fig. 9 Quality factors of $Li_6Mg_7Zr_3O_{16}$-*x* wt% LiF (*x*=1-5) ceramics sintered at 850-1150 °C

Fig. 10 Microwave dielectric properties of the $Li_6Mg_7Zr_3O_{16}$ ceramics doped with 1-5 wt% LiF sintered at 1100 °C

Table caption

Table 1 Phonon parameters obtained from the fitting of the infrared spectra of $Li_6Mg_7Zr_3O_{16}$ ceramic sintered at 1500 °C

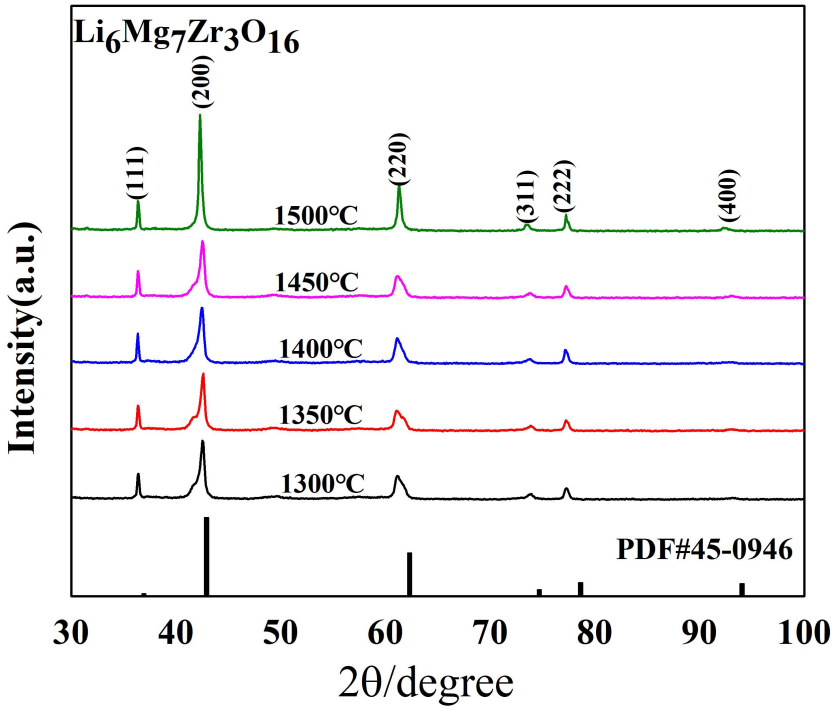
Li6Mg7Zr3O16
(200)
(111)
(220)
(311)
(222)
(400)
1500°C
1450°C
1400°C
1350°C
1300°C
PDF#45-0946
Intensity(a.u.)
30
40
50
60
70
80
90
100
2θ/degree

Fig. 1

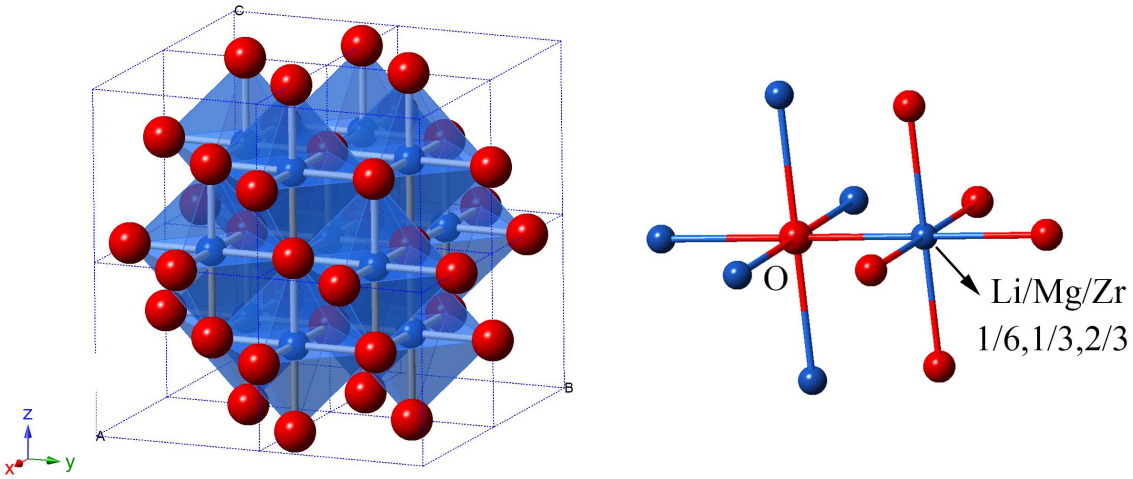

Fig. 2

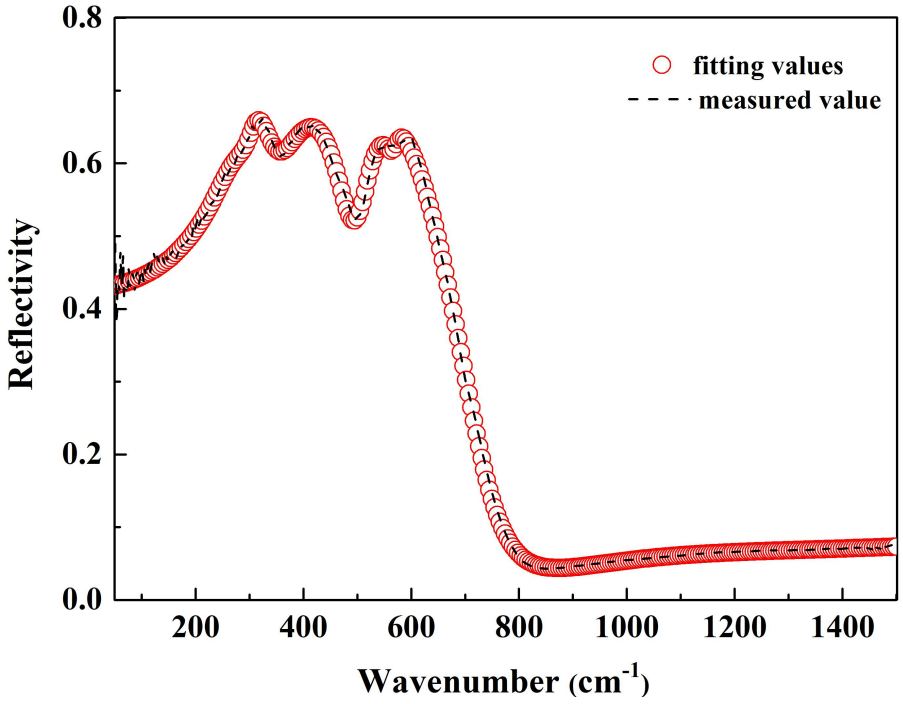
fitting values
measured value
Reflectivity
0.0
0.2
0.4
0.6
0.8
200
400
600
800
1000
1200
1400
Wavenumber (cm-1)

Fig. 3

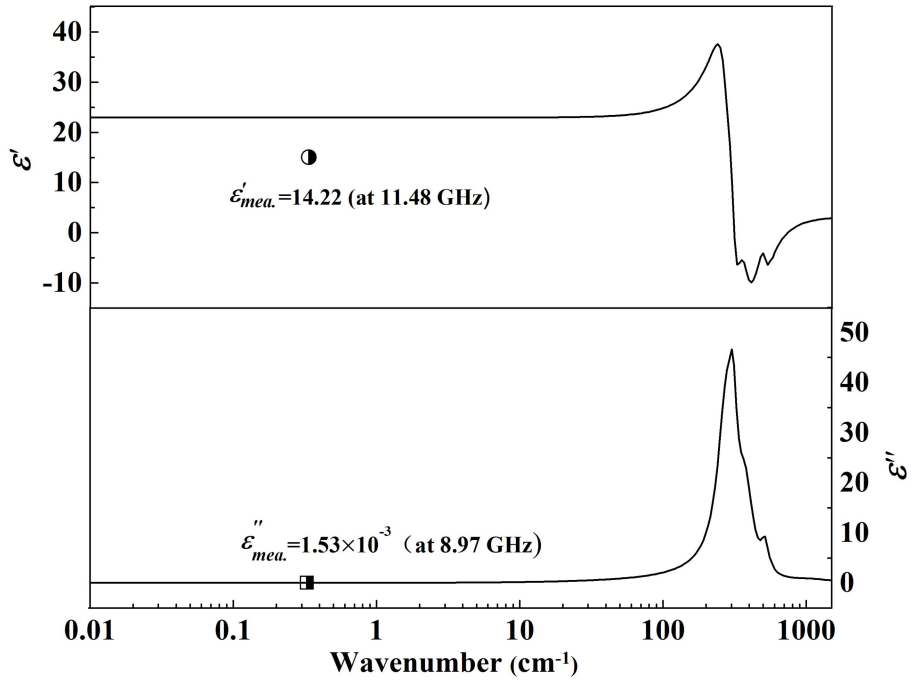
40
30
20
10
0
-10
ε'
ε'mea.=14.22 (at 11.48 GHz)
50
40
30
20
10
0
ε''
ε''mea.=1.53×10-3 (at 8.97 GHz)
0.01
0.1
1
10
100
1000
Wavenumber (cm-1)

Fig. 4

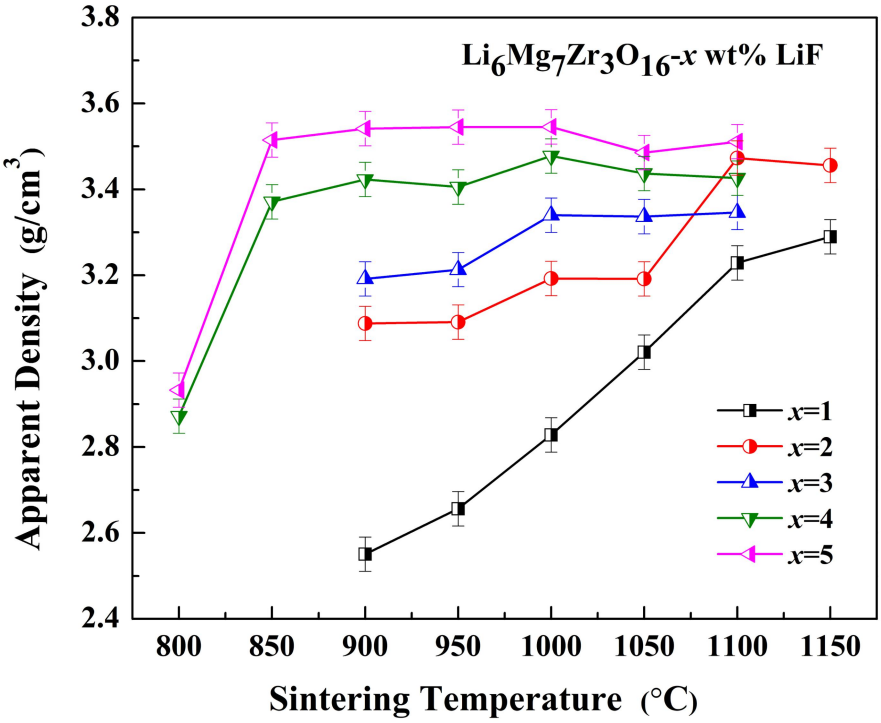
Li6Mg7Zr3O16-x wt% LiF
Apparent Density (g/cm3)
Sintering Temperature (°C)
3.8
3.6
3.4
3.2
3.0
2.8
2.6
2.4
800
850
900
950
1000
1050
1100
1150
x=1
x=2
x=3
x=4
x=5

Fig. 5

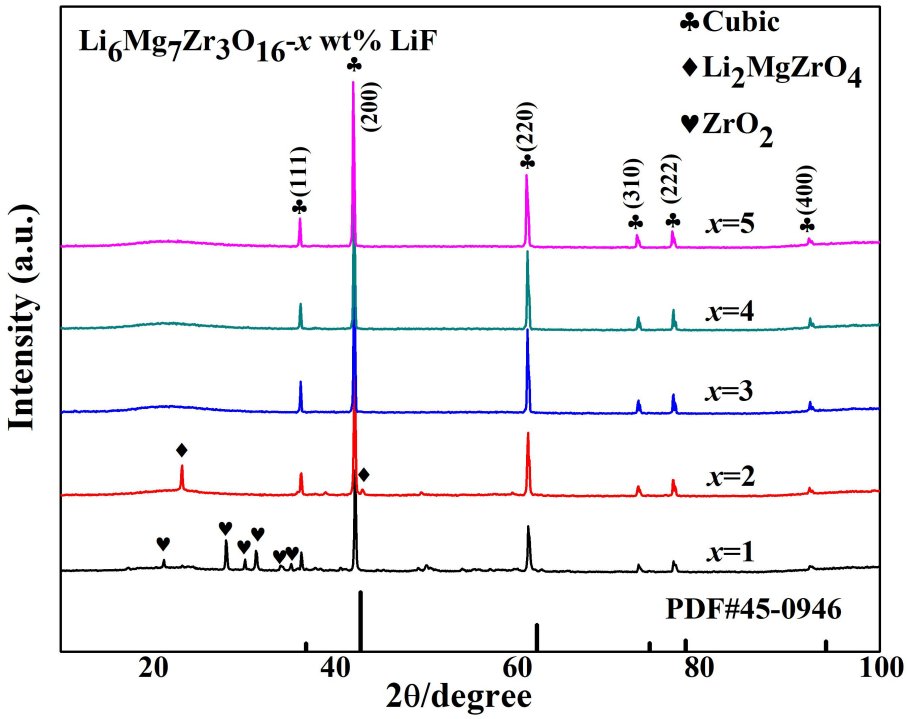
Li6Mg7Zr3O16-x wt% LiF
♣Cubic
♦Li2MgZrO4
♥ZrO2
♣(111)
♣(200)
♣(220)
♣(310)
♣(222)
♣(400)
x=5
x=4
x=3
x=2
x=1
PDF#45-0946
Intensity (a.u.)
20
40
60
80
100
2θ/degree

Fig. 6

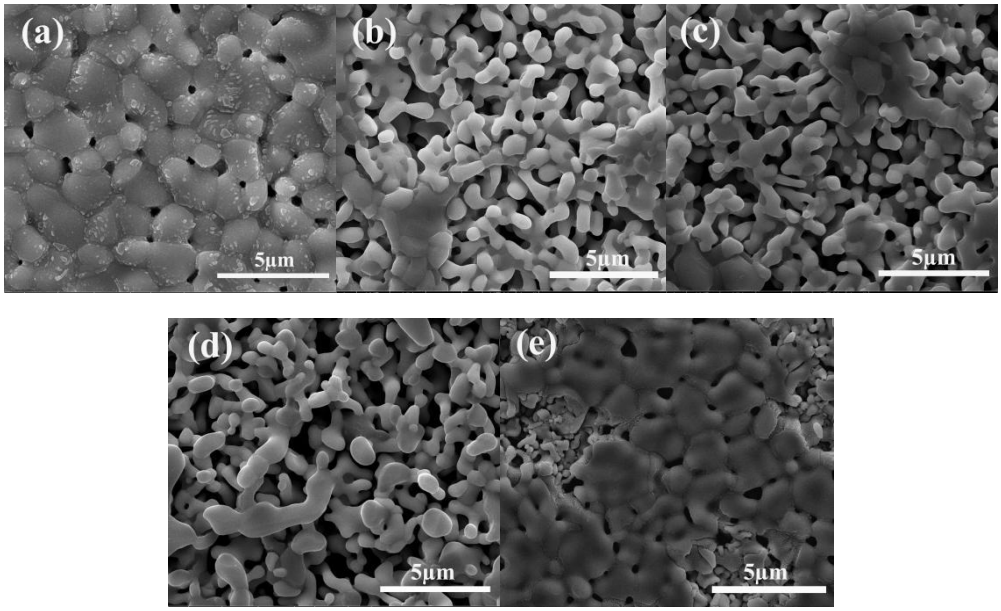

Fig. 7

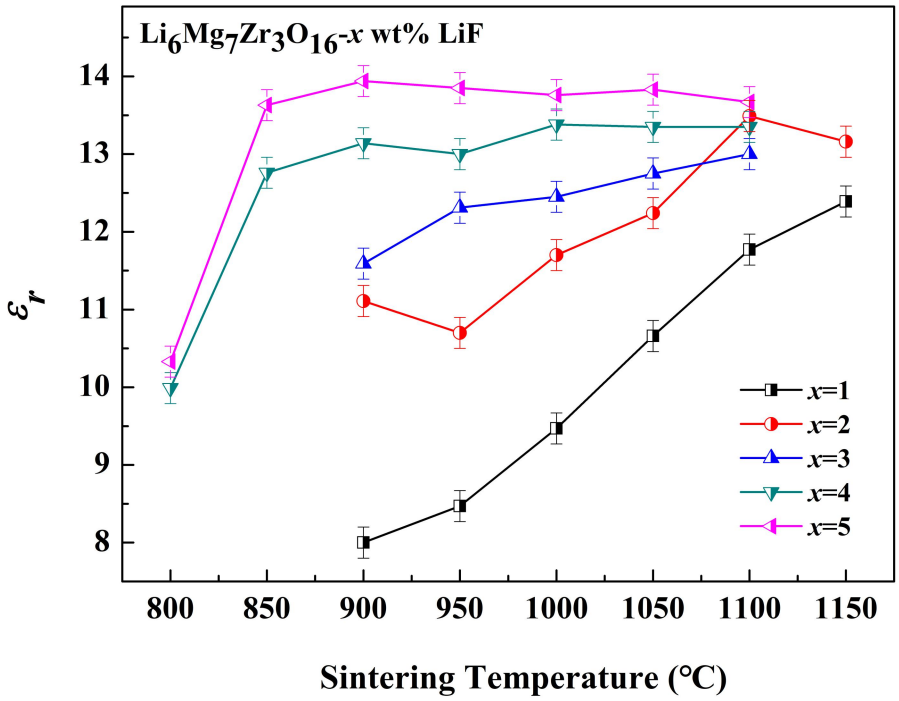
Li6Mg7Zr3O16-x wt% LiF
εr
14
13
12
11
10
9
8
800
850
900
950
1000
1050
1100
1150
Sintering Temperature (°C)
x=1
x=2
x=3
x=4
x=5

Fig. 8

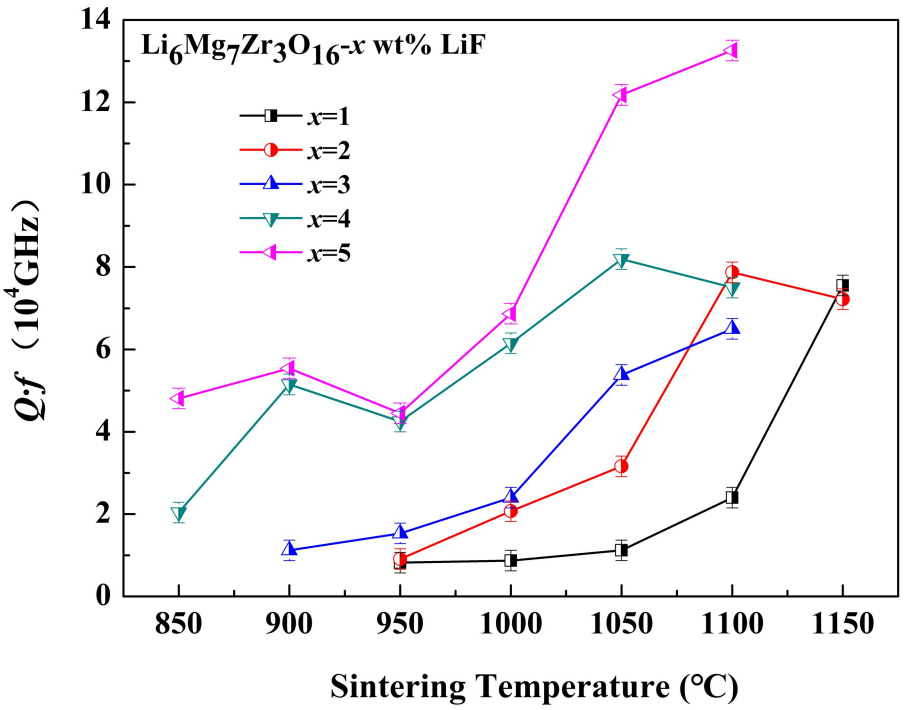
Li6Mg7Zr3O16-x wt% LiF
x=1
x=2
x=3
x=4
x=5
Q·f（10^4GHz）
Sintering Temperature (℃)
0
2
4
6
8
10
12
14
850
900
950
1000
1050
1100
1150

Fig.9

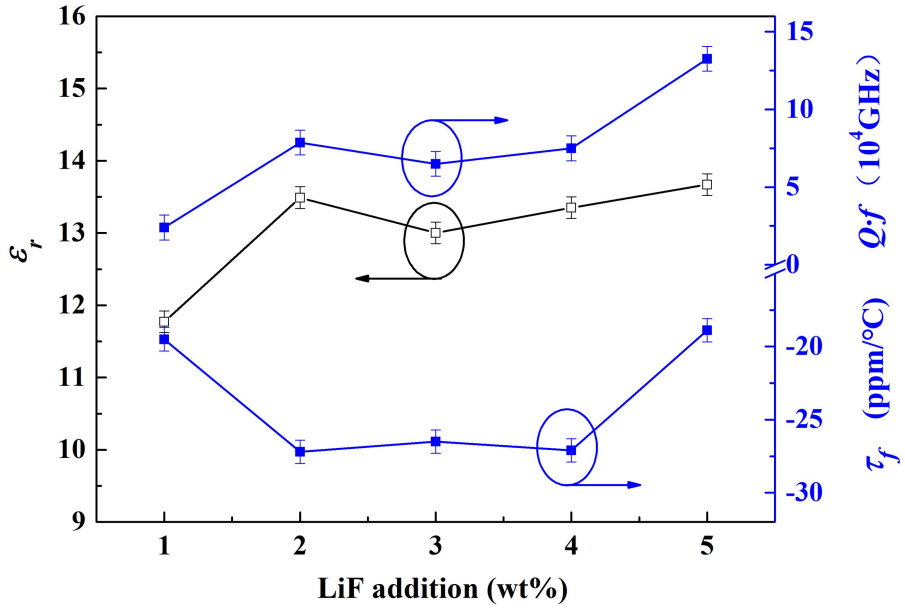
16
15
14
13
12
11
10
9
ε_r
15
10
5
0
-20
-25
-30
$Q{\cdot}f$（10^4GHz）
τ_f (ppm/°C)
1
2
3
4
5
LiF addition (wt%)

Fig. 10

Table 1

mode	ω_{oj}	ω_{pj}	γ_j	$\Delta_{\varepsilon j}$	ε_∞	$\varepsilon^*(\omega)$
1	277.41	855.9	86.452	9.52	4.06	22.88
2	308.73	517.36	44.705	2.81		
3	378.39	855.4	118.34	5.11		
4	513.88	440.03	69.187	0.733		
5	1206.1	973.42	1173.3	0.651		